Molecular-orientation-dependent interference and plateau structures in strong-field ionization of a diatomic molecule by a corotating bichromatic elliptically polarized laser field

M. Busuladžić,[1,2] A. Čerkić,[2] A. Gazibegović-Busuladžić,[2] E. Hasović,[2] and D. B. Milošević[2,3,4]
[1]*Faculty of Medicine, University of Sarajevo, Čekaluša 90, 71000 Sarajevo, Bosnia and Herzegovina*
[2]*Faculty of Science, University of Sarajevo, Zmaja od Bosne 35, 71000 Sarajevo, Bosnia and Herzegovina*
[3]*Academy of Sciences and Arts of Bosnia and Herzegovina, Bistrik 7, 71000 Sarajevo, Bosnia and Herzegovina*
[4]*Max-Born-Institut, Max-Born-Strasse 2a, 12489 Berlin, Germany*

(Received 1 June 2018; published 17 July 2018)

We investigate strong-field ionization of homonuclear diatomic molecules, exemplified with the N_2 molecule, by a bichromatic elliptically polarized laser field having corotating components. We assume that both the emitted electron momentum vector and the internuclear vector of the diatomic molecule lay in the laser-field polarization plane. Our analysis of the low-energy electron spectra caused by the direct above-threshold ionization (ATI) and of the high-energy rescattered electron spectra that can form an extended plateau (high-order ATI or HATI) is based on the improved molecular strong-field approximation. The photoelectron spectra obtained by (H)ATI of molecular targets are more complex and have a reacher structure in comparison to the analogous spectra for atomic targets. We explain the observed interference structures by the interference of two electron wave packets emitted from the two centers of the diatomic molecule. Particular attention is devoted to the HATI spectra. For small values of the ellipticity the photoelectron spectra exhibit a plateau whose length can be as high as $17U_p$, with U_p the electron ponderomotive energy. The yield of high-energy electrons emitted nearly antiparallel to the semimajor axis of the laser-field polarization ellipse is one order of magnitude higher for perpendicular than for the parallel molecular orientation.

DOI: 10.1103/PhysRevA.98.013413

I. INTRODUCTION

Atomic and molecular processes in a strong laser field have been extensively studied in the past few decades. Above-threshold ionization is one of these processes that has attracted a lot of attention in the research community (see review articles [1–4] and references therein). In the first step of this process, the exposed atomic or molecular system absorbs more photons from the laser field than is necessary for ionization [5]. The electron that is released from the atom or molecule by absorbing these photons can go directly to the detector. This process is known as the direct above-threshold ionization (ATI). The released electron is driven by the laser field and may return to the parent atomic or molecular ion (second step). The returned electron may elastically scatter off this ion (third step) before reaching the detector. In this way, many more photons may be absorbed from the laser field than in the direct ATI process. The above-described three-step process is referred to as high-order ATI or HATI [6]. The electrons scattered in the HATI process contribute to the high-energy part of the electron spectrum, forming a plateau in which the (HATI) photoelectron yield is practically constant, but lower than that of the ATI. This plateau is followed by an abrupt cutoff.

Various nonlinear processes generated by strong bichromatic elliptically polarized laser fields have been among the most popular phenomena within the laser science and strong-field physics in the last few years. A special case of bichromatic elliptically polarized laser field is the so-called bicircular field that consists of two coplanar corotating or counterrotating circularly polarized fields having different angular frequencies. Laser-induced process of generation of high-order harmonics by such counterrotating bicircular field was first considered in papers published more than 20 years ago [7–9]. This process was explained using the strong-field approximation (SFA) and quantum-orbit theory in Ref. [10]. Experimental confirmation that the so-generated high harmonics are circularly polarized [11] has triggered investigation of atomic and molecular processes in such fields. In addition to high-order harmonic generation (HHG) (see, for example, Refs. [12–14]), other strong-field processes in bicircular field have also been explored (for reviews see Refs. [15,16]). Examples are above-threshold detachment [17], (H)ATI [18–23], laser-assisted electro-ion radiative recombination [24], laser-assisted scattering [25], nonsequential double ionization [26,27], electron vortices in photoionization [28,29], spin-dependent effects [30], subcycle interference effects [31], high harmonics from relativistic plasmas [32], optical chirality in nonlinear optics [33], attoclock photoelectron interferometry with two-color corotating circular fields [34], and strong-field photoelectron holography of atoms by bicircular two-color laser pulses [35].

Molecular HHG process induced by a bicircular laser field was investigated in Refs. [36–42]. Very few papers are devoted to the molecular HATI generated by bicircular laser field. In Ref. [43], we extended our theoretical approach from the atomic HATI by counterrotating bicircular field to the HATI from molecular targets. In the present paper we analyze HATI of homonuclear diatomic molecules in a corotating bichromatic elliptically polarized laser field. We do not restrict ourselves to a two-component circularly polarized laser field, but rather investigate the cases of various ellipticities

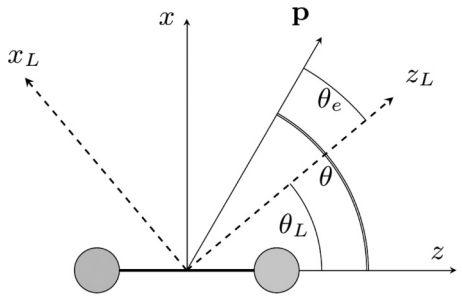

FIG. 1. Schematic presentation of the coordinate systems used in the paper. The two circles along the z axis represent the atomic centers of the diatomic molecule in the zx coordinate system. The laser field is defined in the $z_L x_L$ coordinate system. The ionized electron is emitted with the momentum $\mathbf{p}$ whose direction is determined by the angle θ (θ_e) with respect to the z (z_L) axis.

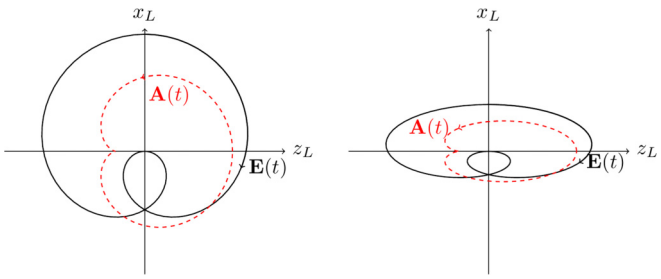

FIG. 2. Normalized electric-field vector $\mathbf{E}(t)$ (solid black lines) and vector potential $\mathbf{A}(t)$ (dashed red lines) of the corotating ω–2ω elliptically polarized laser field (1) for equal component intensities, plotted for $0 \leqslant t \leqslant T$, $T = 2\pi/\omega$. The electric-field vector starts from the point $\mathbf{E}(0) = (0, 0)$ and develops in the clockwise direction for $t > 0$, while the vector potential develops in the counterclockwise direction. The ellipticities of the corotating laser-field components are equal ($\varepsilon_1 = \varepsilon_2 = \varepsilon$) and $\varepsilon = 1$ (left panel) and $\varepsilon = 0.4$ (right panel).

of the corotating field components. A particular attention is devoted to the appearance of the high-energy plateau, which is absent for corotating bicircular fields. Compared with a linearly polarized laser field, for which such plateau exists, many more control parameters are available in a bichromatic elliptically polarized laser field, such as component intensities, frequencies, and ellipticities. As molecules are multicenter systems, it is reasonable to expect that their exposure to a bichromatic elliptically polarized laser field will lead to interesting phenomena.

This paper is organized as follows. In Sec. II we shortly present the improved molecular SFA theory for diatomic molecules in a bichromatic elliptically polarized laser field. The obtained numerical results are presented in Sec. III, while our conclusions are summarized in Sec. IV. We use the atomic system of units ($\hbar = e = m_e = 4\pi\varepsilon_0 = 1$).

II. THEORY AND THE GEOMETRY OF THE PROCESS

Our molecular SFA (MSFA) theory of strong-field ionization of molecular systems was introduced in a series of papers [44–46] (see Ref. [47] for a general case of polyatomic molecules and more references). This theory was confirmed by comparison with the experiments [48–50]. In the present paper we will use the same notation as in Ref. [43] in which our MSFA theory was generalized to the case of bicircular field. More precisely, we suppose that the laser field, the molecule, and the emitted electron all lay in the same plane. The internuclear vector $\mathbf{R}$ of the diatomic molecule is along the z axis. The laser field is defined in the coordinate system $z_L x_L$, which is rotated with respect to the zx coordinate system (defined by the unit vectors $\hat{\mathbf{z}}$ and $\hat{\mathbf{x}}$) by the angle θ_L around the $y = y_L$ axis that is perpendicular to the polarization plane. The direction of the emitted electron momentum $\mathbf{p}$ is determined by the angles θ and θ_e in the zx and $z_L x_L$ coordinate system, respectively (see Fig. 1).

We suppose that the laser field is bichromatic and elliptically polarized having corotating components of frequencies ω and 2ω, with the electric field vector

$$\mathbf{E}(t) = \sum_{j=1}^{2} \frac{E_j}{\sqrt{1+\varepsilon_j^2}} [\hat{\mathbf{e}}_{\mathrm{Lz}} \sin(j\omega t) - \hat{\mathbf{e}}_{\mathrm{Lx}} \varepsilon_j \cos(j\omega t)], \quad (1)$$

where $E_j = I_j^{1/2}$, I_j, and ε_j are the electric field amplitude, intensity, and ellipticity of the jth field component. The fundamental angular frequency is ω and the relative phase between the two corotating field components is fixed to zero. The unit polarization vectors along the z_L and x_L axes are $\hat{\mathbf{e}}_{\mathrm{Lz}} = \hat{\mathbf{z}} \cos\theta_L + \hat{\mathbf{x}} \sin\theta_L$ and $\hat{\mathbf{e}}_{\mathrm{Lx}} = -\hat{\mathbf{z}} \sin\theta_L + \hat{\mathbf{x}} \cos\theta_L$.

The T-matrix element of the (H)ATI process in which the energy $n\omega$ is absorbed from the laser field is

$$T_{\mathbf{R}\mathbf{p}i}(n) = \int_0^T \frac{dt}{T} \mathcal{F}_{\mathbf{R}\mathbf{p}i}(t) e^{i[\mathbf{p}\cdot\boldsymbol{\alpha}(t) + \int^t d\tau \mathbf{A}^2(\tau)/2 + n\omega t - U_{\mathrm{p}} t]}, \quad (2)$$

with the T-periodic functions $\mathcal{F}_{\mathbf{R}\mathbf{p}i}(t)$, $\boldsymbol{\alpha}(t) = \int^t d\tau \mathbf{A}(\tau)$, and $\mathbf{A}(t) = -\int^t d\tau \mathbf{E}(\tau)$, and with $U_{\mathrm{p}} = U_{\mathrm{p}1} + U_{\mathrm{p}2} = E_1^2/(4\omega^2) + E_2^2/(16\omega^2)$ the ponderomotive energy. The normalized electric-field vector $\mathbf{E}(t)$ and the vector potential $\mathbf{A}(t)$ for equal intensities of the corotating laser-field components are presented in Fig. 2. The energy-conservation condition is $n\omega = E_{\mathbf{p}} + U_{\mathrm{p}} + I_{\mathrm{p}}$, where $E_{\mathbf{p}} = \mathbf{p}^2/2$ is the photoelectron kinetic energy and I_{p} is the ionization potential of the molecule.

The zeroth-order term of the MSFA, which corresponds to the direct ATI electrons, within the dressed MSFA in length gauge [44], is described by the matrix element

$$\mathcal{F}^{(0)}_{\mathbf{R}\mathbf{p}i}(t) = \sum_{q=\pm1} e^{iq\mathbf{p}\cdot\mathbf{R}/2} \langle \mathbf{p} + \mathbf{A}(t) | \mathbf{E}(t)\cdot\mathbf{r} \sum_a c_{qa} |\psi_a\rangle, \quad (3)$$

where $|\psi_a\rangle$ are the Slater-type atomic orbitals in which the ground-state molecular wave function is expanded. The sum over q is the sum over the atomic centers ($q = +1$: left center, $q = -1$: right center). The first-order term (improved MSFA), which corresponds to the rescattered electrons, is given by [45]

$$\mathcal{F}^{(1)}_{\mathbf{R}\mathbf{p}i}(t) = -ie^{-iS_{\mathbf{k}_{\mathrm{st}}}(t)} \int_0^\infty d\tau \left(\frac{2\pi}{i\tau}\right)^{3/2} e^{i[S_{\mathbf{k}_{\mathrm{st}}}(t-\tau) - I_{\mathrm{p}}\tau]} \times \sum_{q,q'=\pm1} V^{q'}_{\mathbf{e},\mathbf{k}_{\mathrm{st}}-\mathbf{p}} e^{i[q\mathbf{k}_{\mathrm{st}} - q'(\mathbf{k}_{\mathrm{st}}-\mathbf{p})]\cdot\mathbf{R}/2} \times \langle \mathbf{k}_{\mathrm{st}} + \mathbf{A}(t-\tau) | \mathbf{r}\cdot\mathbf{E}(t-\tau) \sum_a c_{qa} |\psi_a\rangle, \quad (4)$$

with $\mathbf{k}_{\rm st} = -\int_{t-\tau}^{t} dt' \mathbf{A}(t')/\tau$ the stationary electron momentum, $S_{\mathbf{k}_{\rm st}}(t) = \int^{t} dt' [\mathbf{k}_{\rm st} + \mathbf{A}(t')]^2/2$, and $V^{q'}_{\mathrm{e},\mathbf{k}_{\rm st}-\mathbf{p}}$ the Fourier transform of the rescattering potential for the q' center ($q' = +1$ corresponds to the left center, while $q' = -1$ corresponds to the right center in Fig. 1; for details see Ref. [45]). We calculate the differential ionization rate $w_{\mathbf{R}pi}(n) = 2\pi p |T_{\mathbf{R}pi}(n)|^2$ by numerical integration over the times t and τ in Eqs. (3) and (4).

III. NUMERICAL RESULTS

We present our numerical results for the corotating bichromatic elliptically polarized laser field and the N_2 molecule used as a target. We first analyze the spectra of direct electrons, Eq. (3), for different ellipticities and molecular orientations. In the next step, we include additional interaction between the released electron and its parent molecular ion using Eq. (4). Special attention is devoted to the laser and molecular parameters at which the high-energy plateau emerges. The geometry used in our calculations is presented in Fig. 1. It is assumed that the ellipticities of the two laser-field components are equal ($\varepsilon_1 = \varepsilon_2 = \varepsilon$). The ω–2ω elliptically polarized laser field component intensities are $I_1 = I_2 = I = 10^{14}$ W/cm^2 and the fundamental wavelength is 800 nm. We have checked that all features of the spectra shown in this paper are present in a wide range of laser intensities and wavelengths.

A. Direct ATI

In Fig. 3 we present the logarithm of the differential ionization rate in false colors in the electron momentum plane for the direct ATI and the molecular orientation angle $\theta_L = 0^\circ$, 45°, and 90°. For $\theta_L = 0^\circ$ the internuclear axis is along the semimajor axis of the polarization ellipse (see Fig. 1) and the orientation of the molecule is parallel. For $\theta_L = 90^\circ$ the orientation is perpendicular. The spectra shown in the left and right panels of Fig. 3 are calculated for $\varepsilon = 1$ and $\varepsilon = 0.4$, respectively. Let us explain the shape of the presented direct ATI spectra. The integral over the ionization time t in Eqs. (2) and (3) can be solved using the saddle-point method which leads to the nonlinear equation for the ionization time [17]: $[\mathbf{p} + \mathbf{A}(t)]^2 = -2I_{\rm p}$. If we neglect the ionization potential $I_{\rm p}$ in this equation, we obtain that the electrons are predominantly emitted opposite to the direction of the vector potential at the ionization time, i.e., $\mathbf{p} = -\mathbf{A}(t)$. Therefore, the emission in the direction determined by $-\mathbf{A}(t)$ has the key influence on the ATI spectra, i.e., it determines the dominant feature of the spectra (compare Fig. 2 and the top panels of Fig. 3).

The spectra presented in the top and bottom panels of Fig. 3 obey the reflection symmetry with respect to the p_z axis, i.e., the ionization rates are the same for the angles θ_e and $360^\circ - \theta_e$. This reflection symmetry was analyzed in detail for the counterrotating bicircular field, both for atoms [19] and molecules [43]. However, for corotating bichromatic elliptically polarized laser field this $\theta_e \to 360^\circ - \theta_e$ symmetry is satisfied only for the parallel and perpendicular orientations of the homonuclear diatomic molecules, while it is absent for other molecular orientations, as it can be seen from the middle panels of Fig. 3.

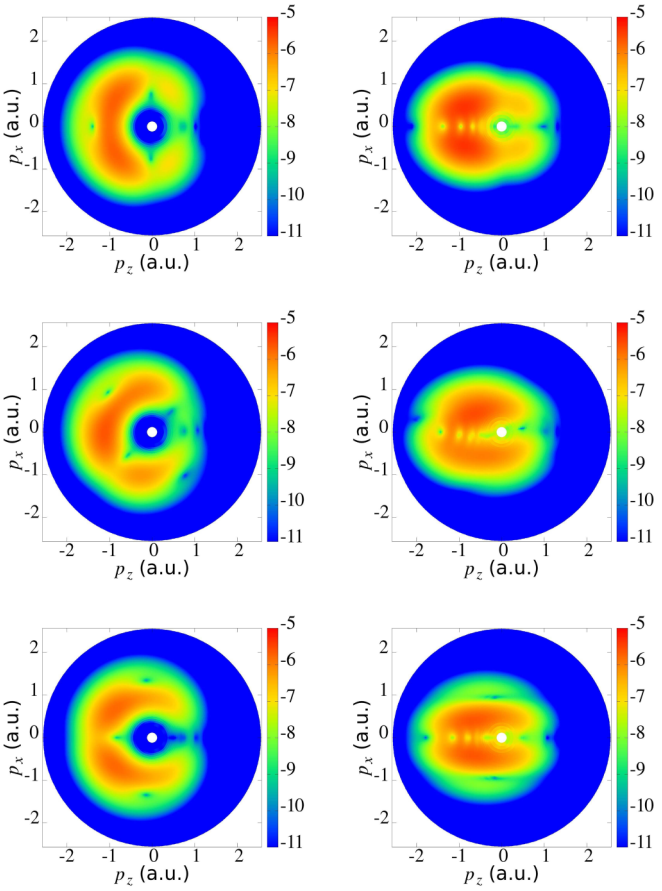

FIG. 3. Direct ATI electron spectra obtained using the MSFA for the N_2 molecule. The intensities of the ω–2ω corotating laser-field components are 10^{14} W/cm^2 and the fundamental wavelength is 800 nm. The electron momentum plane is defined with respect to the laser-field coordinate system: $p_z = p\cos\theta_e$, $p_x = p\sin\theta_e$. The angle between the internuclear axis and the semimajor axis of the laser-field polarization ellipse is $\theta_L = 0^\circ$ (top panels, parallel orientation), $\theta_L = 45^\circ$ (middle panels), and $\theta_L = 90^\circ$ (bottom panels, perpendicular orientation). The ellipticities of the laser field are $\varepsilon = 1$ (left panels) and $\varepsilon = 0.4$ (right panels). The false color scale covers six orders of magnitude. Results are presented for $E_{\mathbf{p}} \leqslant 12U_{\rm p}$.

In addition, all spectra presented in Fig. 3 are characterized by the two-center destructive interference minima. The phase difference between the two electron wave packets emitted from the left center ($q = +1$) and the right center ($q = -1$) is $\mathbf{p}\cdot\mathbf{R} = pR\cos\theta$. The interference of these wave packets is destructive if $pR\cos\theta = (2m+1)\pi$, with m integer. For $m = 0$, $R = 2.068$ a.u. (equilibrium internuclear distance of the used N_2 molecule), $\theta_L = 0^\circ$, and $\theta \approx 180^\circ$ (for the top left panel of Fig. 3 we have $\theta_e = \theta - \theta_L = \theta$) the minimum appears at $p_z \approx -1.5$ a.u. The above simple destructive interference condition should be modified taking into account the molecular symmetry. It can be shown [45] that in Eq. (3) the coefficients c_{qa} satisfy the relation $c_{-1a} = s_{a\lambda}c_{1a}$, with $s_{a\lambda} = (-1)^{l_a}$ for $3\sigma_g$ highest-occupied molecular orbital of N_2 molecule and l_a the orbital quantum number of the used orbital (12 Slater-type orbitals having $l_a = 0, 1, 2, 3$ are used in our calculations). In this case the summation over q in Eq. (3) gives the

factor

$$e^{i\mathbf{p}\cdot\mathbf{R}/2} + s_{a\lambda}e^{-i\mathbf{p}\cdot\mathbf{R}/2} = \begin{cases} 2\cos(\mathbf{p}\cdot\mathbf{R}/2) & \text{for } s_{a\lambda} = +1, \\ 2i\sin(\mathbf{p}\cdot\mathbf{R}/2) & \text{for } s_{a\lambda} = -1. \end{cases} \quad (5)$$

For $s_{a\lambda} = +1$ the corresponding destructive interference condition is equivalent to the above-described condition for destructive interference of emitted wave packets, $pR\cos\theta = (2m+1)\pi$. For $s_{a\lambda} = -1$ the destructive-interference condition is different. In general, for $s_{a\lambda} = \pm 1$ the corresponding momenta $p_{\mathrm{min},m}^{(s_{a\lambda})}$ are

$$p_{\mathrm{min},m}^{(+1)} = \frac{(2m+1)\pi}{R\cos(\theta_e - \theta_L)}, \quad p_{\mathrm{min},m}^{(-1)} = \frac{2(m+1)\pi}{R\cos(\theta_e - \theta_L)}, \quad (6)$$

where $m = 0, \pm 1, \pm 2, \ldots$. For the used laser and molecular parameters the minima which correspond to $p_{\mathrm{min},0}^{(+1)}$ and $p_{\mathrm{min},-1}^{(-1)}$ are clearly visible in the top left panel of Fig. 3. If we take into account only the orbitals with l_a even, the interference minima form a straight line $p_z = p_{\mathrm{min},0}^{(+1)}\cos(\theta_e - \theta_L) = -\pi/R$ in the momentum plane. Analogously, for l_a odd we have $p_z = p_{\mathrm{min},-1}^{(-1)}\cos(\theta_e - \theta_L) = 0$. Since both even and odd orbitals contribute to the spectra, the mentioned minima are partially masked, as it can be seen in the top left panel of Fig. 3. Comparing this result with those presented in other left panels, we see that the positions of the minima are rotated by the angle $-\theta_L$, which is in accordance with Eq. (6). More precisely, while for the top left panel the minimum appears for $\theta_e = 180°$, for the middle left panel ($\theta_L = 45°$) it appears for $\theta_e = 135°$, and for the bottom left panel ($\theta_L = 90°$) it appears for $\theta_e = 90°$.

For the ellipticity $\varepsilon = 0.4$ (right panels of Fig. 3), in addition to the two-center-interference minima, which satisfy relation (6), one can notice series of minima along the p_z axis. We checked that these minima appear at the same places as the interference minima for Ar atoms (for the same laser parameters; Ar atom is companion of the N_2 molecule due to nearly equal ionization potential). Therefore, these minima are caused by the interference of the parts of the wave packet emitted from the same center of the N_2 molecule. For the corotating bicircular field these single-atom interference minima are absent [15,20].

B. Rescattering high-order ATI

We now consider high-energy photoelectron spectra governed by a corotating ω–2ω elliptically polarized laser field. The analysis of the HATI process includes the rescattering of the released electron off the parent molecular ion. In this sense, we calculate the differential ionization rate as a coherent sum of the two terms given by Eqs. (3) and (4). The spectra calculated for different values of the ellipticity and for parallel molecular orientation are presented in Fig. 4. Comparing the top panel of Fig. 4 with the top right panel of Fig. 3 ($\theta_L = 0°$ and $\varepsilon = 0.4$) we see that now the reflection symmetry is violated and that, due to the rescattering effects, long plateaus are developed for high electron energies, both for $\theta_e = 0°$ ($p_z > 2$ a.u.) and for $\theta_e = 180°$ ($p_z < -2$ a.u.). As we will see, the plateau for $\theta_e = 180°$ is even longer. This is not visible in Fig. 4, where we limit our presentation to six orders of magnitude and to the energies lower than $12U_p$ (compare Fig. 8, where the rate is below 10^{-11} a.u. near the cutoff at $16U_p$). From other panels

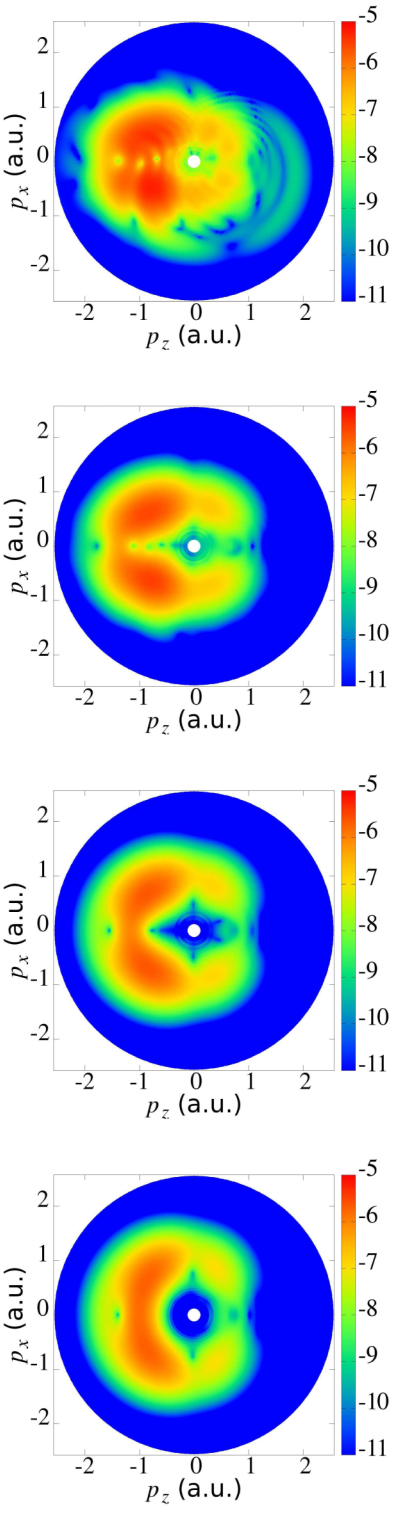

FIG. 4. Electron HATI spectra obtained using the improved MSFA (both the direct and the rescattered electrons are included) for the N_2 molecule and parallel molecular orientation. The four presented momentum distributions correspond to different values of the ellipticity: $\varepsilon = 0.4$, $\varepsilon = 0.6$, $\varepsilon = 0.8$, and $\varepsilon = 1$, from the top to the bottom panel, respectively. The intensities of the ω–2ω corotating laser-field components are 10^{14} W/cm^2 and the fundamental wavelength is 800 nm.

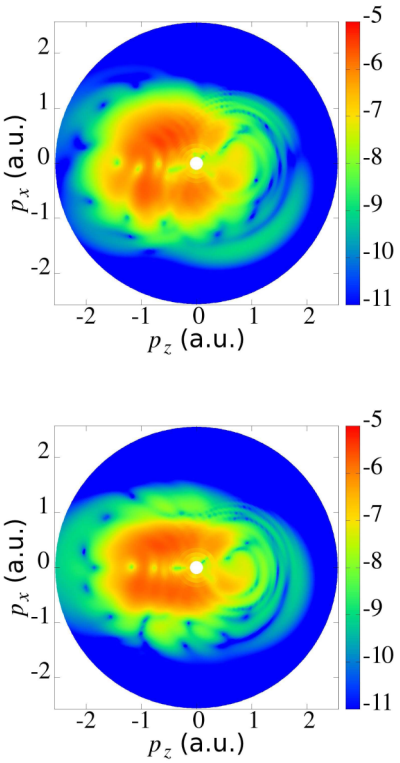

FIG. 5. Same as in Fig. 4 but for the ellipticity $\varepsilon = 0.4$ and the angle of molecular orientation $\theta_L = 45^\circ$ (upper panel) and $\theta_L = 90^\circ$ (lower panel).

of Fig. 4, we see that, with the increase of the ellipticity, the rescattering plateau becomes less visible and disappears for the corotating bicircular laser field ($\varepsilon = 1$). Thus, the rescattering effects are negligible for corotating bicircular laser field. This is the case both for the atomic and for the molecular HATI.

To analyze the contribution of high-energy electrons to the HATI spectra as a function of the molecular orientation, in Fig. 5 we present the summed differential spectra in the electron momentum plane for $\varepsilon = 0.4$ and for $\theta_L = 45^\circ$ and $\theta_L = 90^\circ$ (the case of $\theta_L = 0^\circ$ is already shown in the top panel of Fig. 4). A detailed inspection of these results leads to the conclusion that the structure and the height of the high-energy plateau do not change much in the region around $\theta_e = 0^\circ$ for the parallel and perpendicular molecular orientation, while for $\theta_L = 45^\circ$ there is a significant suppression of the plateau height for $\theta_e \approx 0^\circ$. On the other hand, for $\theta_e = 180^\circ$ there is a considerable difference in the structure (height) of the spectra for the parallel (top panel of Fig. 4) and perpendicular (bottom panel of Fig. 5) molecular orientations. As the value of θ_L increases from $\theta_L = 0^\circ$ (parallel) to $\theta_L = 90^\circ$ (perpendicular orientation) the corresponding yield of the high-energy electrons around $\theta_e = 180^\circ$ becomes higher and more visible. It is an interesting effect that could be observed in future experiments. We will examine this effect in more details.

In the remaining figures we will show only the rescattered (HATI) photoelectron spectra for fixed electron emission angles. In Fig. 6 we show the energy-resolved rescattered photoelectron spectra obtained for parallel molecular orientation, for the corotating ω–2ω laser field, for four different values of the ellipticity, and for the electron emission angle $\theta_e = 0^\circ$. For

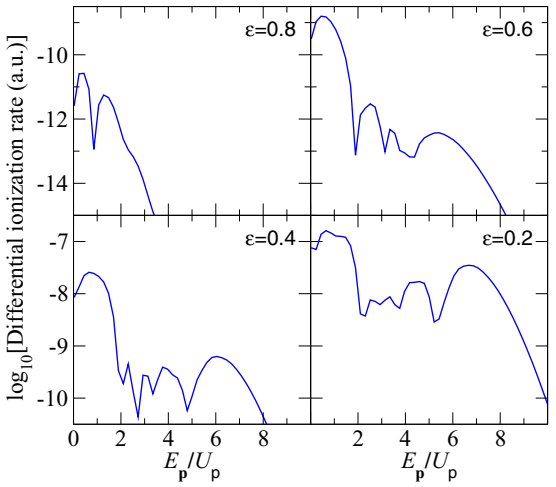

FIG. 6. Rescattered photoelectron energy spectra for the N_2 molecules ionized by a corotating ω–2ω field, obtained for parallel molecular orientation ($\theta_L = 0^\circ$), for various values of the ellipticity ε denoted in the upper right corner of each panel, and for the electron emission angle $\theta_e = 0^\circ$. Other laser parameters are as in Fig. 3.

lower values of the ellipticity, the high-energy plateau is well developed with the cutoff position near $8U_p$ (see, for example, the results for $\varepsilon = 0.2$ in the lower right panel of Fig. 6). As the ellipticity increases, the cutoff of the high-energy plateau shifts to the lower energies and the plateau height (i.e., the high-energy electron yield) decreases. As one can see from the upper right panel of Fig. 6, the rescattering plateau is almost entirely suppressed for $\varepsilon = 0.6$. For even higher values of the ellipticity the rescattering plateau is not observable (compare the upper left panel of Fig. 6, where the results for $\varepsilon = 0.8$ are presented).

Another example of the energy-resolved rescattered photoelectron spectra is presented in Fig. 7 for the electron emission angle $\theta_e = 180^\circ$. One can observe that in this case almost all curves are characterized by a lower probability than those for $\theta_e = 0^\circ$, presented in Fig. 6. In addition, the high-energy plateau for small values of ε is longer for $\theta_e = 180^\circ$ than for $\theta_e = 0^\circ$. Figure 7 shows that the cutoff of the high-energy plateau for $\theta_e = 180^\circ$ is about $16U_p$ for $\varepsilon = 0.2$ and $\varepsilon = 0.4$.

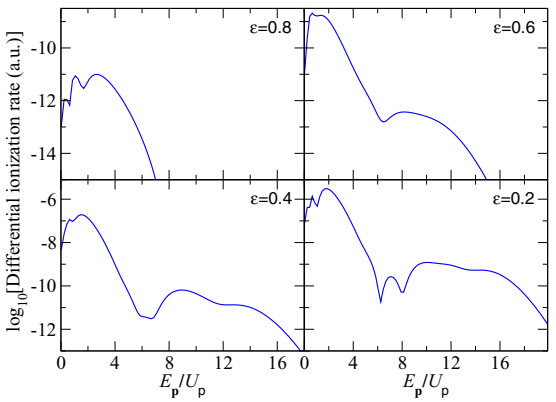

FIG. 7. Same as in Fig. 6 but for the electron emission angle $\theta_e = 180^\circ$.

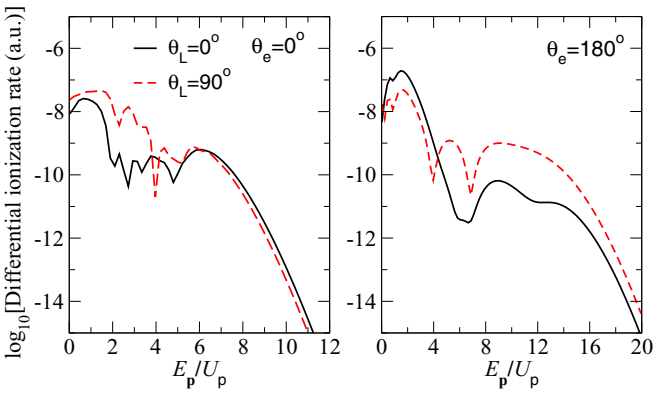

FIG. 8. Rescattered photoelectron energy spectra for the N_2 molecule ionized by a corotating ω–2ω field. The ellipticity of the laser-field components is $\varepsilon = 0.4$, while the electron emission angles are $\theta_e = 0^\circ$ (left panel) and $\theta_e = 180^\circ$ (right panel). The spectra for parallel (black solid lines) and perpendicular (red dashed lines) orientation of the molecule are presented. Other laser parameters are as in Fig. 3.

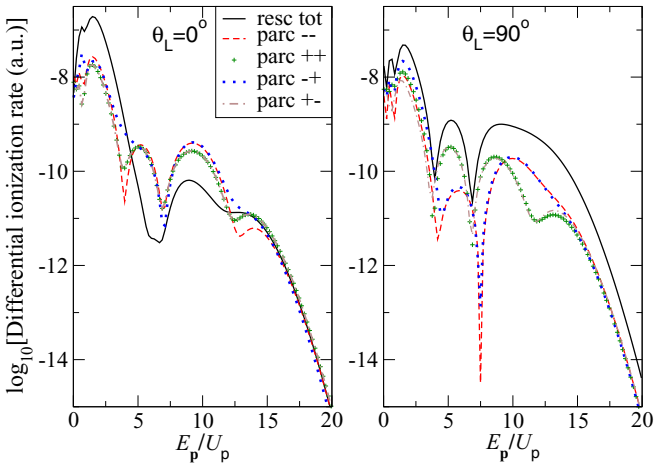

FIG. 10. Total (solid line) and partial differential ionization rates for the N_2 molecule ionized by a corotating ω–2ω field, for the same parameters as in Fig. 8 and for $\theta_e = 180^\circ$. Left panel: $\theta_L = 0^\circ$. Right panel: $\theta_L = 90^\circ$.

This plateau vanishes for higher values of ε, both for $\theta_e = 0^\circ$ and $\theta_e = 180^\circ$.

Finally, we analyze the energy-resolved rescattered photoelectron spectra for the parallel ($\theta_L = 0^\circ$) and perpendicular ($\theta_L = 90^\circ$) orientations, and for two fixed values of the electron emission angle, $\theta_e = 0^\circ$ and $\theta_e = 180^\circ$. The results are presented in Fig. 8. From the left panel of Fig. 8 one can see that for $\theta_e = 0^\circ$ the high-energy electron yields for $\theta_L = 0^\circ$ and $\theta_L = 90^\circ$ are comparable. For $\theta_e = 180^\circ$ the high-energy electron yield calculated for $\theta_L = 90^\circ$ is one order of magnitude higher than that calculated for $\theta_L = 0^\circ$ (see the right panel of Fig. 8). This difference between the high-energy electron yields for $\theta_L = 0^\circ$ and $\theta_L = 90^\circ$ exists for wide ranges of ellipticities, intensities, and wavelengths. In Fig. 9 we show an example of the ellipticity dependence. One should keep in mind that the high-energy plateau is much longer for $\theta_e = 180^\circ$ than for $\theta_e = 0^\circ$, regardless of the molecular orientation (see Fig. 8).

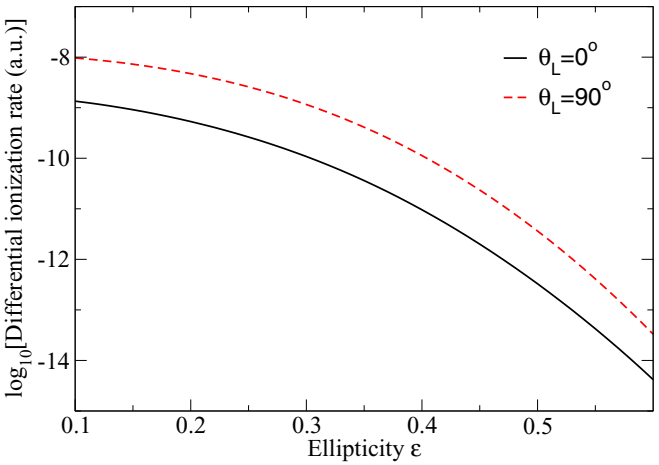

FIG. 9. Differential ionization rate of the N_2 molecule as a function of the ellipticity ε of the laser-field components, for the fixed electron energy of 105 eV ($14U_p$) and for two molecular orientations, $\theta_L = 0^\circ$ (black solid line) and $\theta_L = 90^\circ$ (red dashed line). The electron emission angle is $\theta_e = 180^\circ$. Other laser parameters are as in Fig. 8.

The reason why the rates in the plateau region are higher for the perpendicular than for the parallel orientation is the constructive or destructive interference of partial T-matrix contributions. Namely, the rescattering T-matrix element can be written as $T^R = T^{++} + T^{--} + T^{+-} + T^{-+}$. The terms T^{++} and T^{--} refer to the situation where the electron is born at and rescatters off the same center, while in T^{+-} and T^{-+} these two events take place at different centers. It can be shown [45] that $T^R \propto \cos\gamma$ where $2\gamma = (\mathbf{p} - \mathbf{k}_{st}) \cdot \mathbf{R}$. The rates obtained using partial T-matrix contributions, for the parameters of right panel of Fig. 8, are shown in Fig. 10. For $\theta_e = 180^\circ$ we have $(\mathbf{p} - \mathbf{k}_{st}) \cdot \mathbf{R} = R[k_{xL} \sin\theta_L - (k_{zL} + p)\cos\theta_L]$, where k_{zL} and k_{xL} are the corresponding components of the stationary momentum $\mathbf{k}_{st}$ in the laser field coordinate system. For small ellipticities k_{xL} is also small since $\mathbf{k}_{st} \approx -\mathbf{A}(t_0)$ [compare the right panel of Fig. 2 where $\mathbf{A}(t)$ is presented]. For $\theta_L = 90^\circ$ and small k_{xL} we have $\gamma \approx 0$ so that $\cos\gamma \approx 1$ and we have constructive interference, as can be seen in the right panel of Fig. 10.

IV. CONCLUSION

Using the improved molecular strong-field approximation, we investigate the strong-field ionization of N_2 molecules by a corotating bichromatic (ω–2ω) elliptically polarized laser field. The photoelectron spectra of both the direct (ATI) and the rescattered (HATI) electrons are analyzed. The obtained spectra are more complex than the corresponding atomic (H)ATI spectra. For all considered cases, a destructive interference structure is imprinted into the spectra. We explain this structure by the interference of two electron wave packets emitted from the two centers of the diatomic molecule. The high-energy plateau, characterized by the rescattered electrons, does not appear in the energy spectra obtained by a corotating bicircular laser field, which is a result analogous to that of the atomic HATI.

In the case of molecular direct ATI, the reflection symmetry about the p_z axis (in the laser-field coordinate system) is preserved for the parallel and perpendicular molecular orientations. This symmetry is violated for other orientations, as well as for the HATI spectra which include the rescattering effects. The analysis of the rescattering effects shows that the high-energy plateau can be observed for the ellipticities lower than $\varepsilon = 0.4$. The yield of the rescattered electrons rapidly decreases for higher values of the ellipticities and cannot be observed for $\varepsilon \geqslant 0.6$ (for the molecular orientations we considered: $\theta_L = 0^\circ$, 45°, and 90°). This information can be useful for experimentalists.

For the used bichromatic laser field and for the angle of electron emission around $\theta_e = 180^\circ$ (i.e., nearly antiparallel to the semimajor axis of the laser-field polarization ellipse) the high-energy plateau has maximum length and is much longer than for the spectra obtained using a linearly or an elliptically polarized monochromatic field. The cutoff energy of the plateau can be higher than $16U_\mathrm{p}$ for small values of the ellipticity. In the limit of $\varepsilon \to 0$ the classical cutoff tends to $16.72U_\mathrm{p}$ as in the case of an ω–2ω linearly polarized laser field [51,52] (in these papers the calculated classical cutoff was $20.9U_{\mathrm{p}1}$).

An important contribution of this paper is the prediction of a strong molecular orientation dependence of the HATI spectra for $\theta_e \approx 180^\circ$. As the value of θ_L increases from the parallel ($\theta_L = 0^\circ$) to the perpendicular ($\theta_L = 90^\circ$) orientation, the corresponding yield of high-energy electrons around $\theta_e = 180^\circ$ increases by at least one order of magnitude. This effect occurs for $\varepsilon \leqslant 0.4$ and can be useful for determination or control of the molecular orientation in experiments. We have checked that this effect exists for a wide range of the laser field intensities and wavelengths.

[1] W. Becker, F. Grasbon, R. Kopold, D. B. Milošević, G. G. Paulus, and H. Walther, Adv. At. Mol. Opt. Phys. **48**, 35 (2002).
[2] A. Becker and F. H. M. Faisal, J. Phys. B **38**, R1 (2005).
[3] M. Lein, J. Phys. B **40**, R135 (2007).
[4] L. F. DiMauro and P. Agostini, Adv. At. Mol. Opt. Phys. **61**, 117 (2012).
[5] P. Agostini, F. Fabre, G. Mainfray, G. Petite, and N. K. Rahman, Phys. Rev. Lett. **42**, 1127 (1979).
[6] G. G. Paulus, W. Nicklich, H. Xu, P. Lambropoulos, and H. Walther, Phys. Rev. Lett. **72**, 2851 (1994).
[7] H. Eichmann, A. Egbert, S. Nolte, C. Momma, B. Wellegehausen, W. Becker, S. Long, and J. K. McIver, Phys. Rev. A **51**, R3414 (1995).
[8] S. Long, W. Becker, and J. K. McIver, Phys. Rev. A **52**, 2262 (1995).
[9] T. Zuo and A. D. Bandrauk, J. Nonlin. Opt. Phys. Mater. **04**, 533 (1995).
[10] D. B. Milošević, W. Becker, and R. Kopold, Phys. Rev. A **61**, 063403 (2000).
[11] A. Fleischer, O. Kfir, T. Diskin, P. Sidorenko, and O. Cohen, Nat. Photon. **8**, 543 (2014).
[12] T. Fan *et al.*, Proc. Natl. Acad. Sci. USA **112**, 14206 (2015).
[13] C. Chen *et al.*, Sci. Adv. **2**, e1501333 (2016).
[14] J. Heslar, D. A. Telnov, and S.-I. Chu, Phys. Rev. A **97**, 043419 (2018).
[15] S. Odžak, E. Hasović, W. Becker, and D. B. Milošević, J. Mod. Opt. **64**, 971 (2017).
[16] A. D. Bandrauk, J. Guo, and K.-J. Yuan, J. Opt. **19**, 124016 (2017).
[17] A. Kramo, E. Hasović, D. B. Milošević, and W. Becker, Laser Phys. Lett. **4**, 279 (2007); E. Hasović, A. Kramo, and D. B. Milošević, Eur. Phys. J. Special Topics **160**, 205 (2008).
[18] C. A. Mancuso, D. D. Hickstein, P. Grychtol, R. Knut, O. Kfir, X. M. Tong, F. Dollar, D. Zusin, M. Gopalakrishnan, C. Gentry, E. Turgut, J. L. Ellis, M. C. Chen, A. Fleischer, O. Cohen, H. C. Kapteyn, and M. M. Murnane, Phys. Rev. A **91**, 031402(R) (2015).
[19] E. Hasović, W. Becker, and D. B. Milošević, Opt. Express **24**, 6413 (2016); D. B. Milošević and W. Becker, Phys. Rev. A **93**, 063418 (2016).
[20] C. A. Mancuso, D. D. Hickstein, K. M. Dorney, J. L. Ellis, E. Hasović, R. Knut, P. Grychtol, C. Gentry, M. Gopalakrishnan, D. Zusin, F. J. Dollar, X. M. Tong, D. B. Milošević, W. Becker, H. C. Kapteyn, and M. M. Murnane, Phys. Rev. A **93**, 053406 (2016).
[21] V.-H. Hoang, V.-H. Le, C. D. Lin, and A.-T. Le, Phys. Rev. A **95**, 031402(R) (2017).
[22] D. B. Milošević and W. Becker, J. Phys. B **51**, 054001 (2018).
[23] A. Gazibegović-Busuladžić, W. Becker, and D. B. Milošević, Opt. Express **26**, 12684 (2018).
[24] S. Odžak and D. B. Milošević, Phys. Rev. A **92**, 053416 (2015); A. Čerkić, M. Busuladžić, and D. B. Milošević, *ibid.* **95**, 063401 (2017).
[25] A. Korajac, D. Habibović, A. Čerkić, M. Busuladžić, and D. B. Milošević, Eur. Phys. J. D **71**, 251 (2017).
[26] C. A. Mancuso, K. M. Dorney, D. D. Hickstein, J. L. Chaloupka, J. L. Ellis, F. J. Dollar, R. Knut, P. Grychtol, D. Zusin, C. Gentry, M. Gopalakrishnan, H. C. Kapteyn, and M. M. Murnane, Phys. Rev. Lett. **117**, 133201 (2016).
[27] S. Eckart, M. Richter, M. Kunitski, A. Hartung, J. Rist, K. Henrichs, N. Schlott, H. Kang, T. Bauer, H. Sann, L. P. H. Schmidt, M. Schoffler, T. Jahnke, and R. Dorner, Phys. Rev. Lett. **117**, 133202 (2016).
[28] J. M. Ngoko Djiokap, S. X. Hu, L. B. Madsen, N. L. Manakov, A. V. Meremianin, and A. F. Starace, Phys. Rev. Lett. **115**, 113004 (2015).
[29] D. Pengel, S. Kerbstadt, D. Johannmeyer, L. Englert, T. Bayer, and M. Wollenhaupt, Phys. Rev. Lett. **118**, 053003 (2017).
[30] D. B. Milošević, Phys. Rev. A **93**, 051402(R) (2016); J. Phys. B **50**, 164003 (2017).
[31] S. Eckart, M. Kunitski, I. Ivanov, M. Richter, K. Fehre, A. Hartung, J. Rist, K. Henrichs, D. Trabert, N. Schlott, L. P. H. Schmidt, T. Jahnke, M. S. Schoffler, A. Kheifets, and R. Dorner, Phys. Rev. A **97**, 041402(R) (2018).
[32] Z.-Y. Chen, Phys. Rev. E **97**, 043202 (2018).
[33] O. Neufeld and O. Cohen, Phys. Rev. Lett. **120**, 133206 (2018).
[34] M. Han, P. Ge, Y. Shao, Q. Gong, and Y. Liu, Phys. Rev. Lett. **120**, 073202 (2018).

[35] M. Li, W.-C. Jiang, H. Xie, S. Luo, Y. Zhou, and P. Lu, Phys. Rev. A **97**, 023415 (2018).
[36] D. Baykusheva, M. S. Ahsan, N. Lin, and H. J. Wörner, Phys. Rev. Lett. **116**, 123001 (2016).
[37] F. Mauger, A. D. Bandrauk, and T. Uzer, J. Phys. B **49**, 10LT01 (2016).
[38] H. Du, J. Zhang, S. Ben, H.-Y. Zhong, T.-T. Xu, J. Guo, and X.-S. Liu, Chin. Phys. B **25**, 043202 (2016).
[39] X. Liu, X. Zhu, L. Li, Y. Li, Q. Zhang, P. Lan, and P. Lu, Phys. Rev. A **94**, 033410 (2016).
[40] S. Odžak, E. Hasović, and D. B. Milošević, Phys. Rev. A **94**, 033419 (2016).
[41] D. M. Reich and L. B. Madsen, Phys. Rev. Lett. **117**, 133902 (2016).
[42] E. Hasović, S. Odžak, W. Becker, and D. B. Milošević, Mol. Phys. **115**, 1750 (2017).
[43] M. Busuladžić, A. Gazibegović-Busuladžić, and D. B. Milošević, Phys. Rev. A **95**, 033411 (2017); A. Gazibegović-Busuladžić, M. Busuladžić, E. Hasović, W. Becker, and D. B. Milošević, *ibid.* **97**, 043432 (2018).
[44] D. B. Milošević, Phys. Rev. A **74**, 063404 (2006).
[45] M. Busuladžić, A. Gazibegović-Busuladžić, D. B. Milošević, and W. Becker, Phys. Rev. Lett. **100**, 203003 (2008); Phys. Rev. A **78**, 033412 (2008).
[46] M. Busuladžić, A. Gazibegović-Busuladžić, and D. B. Milošević, Phys. Rev. A **80**, 013420 (2009).
[47] E. Hasović and D. B. Milošević, Phys. Rev. A **89**, 053401 (2014).
[48] M. Okunishi, R. Itaya, K. Shimada, G. Prümper, K. Ueda, M. Busuladžić, A. Gazibegović-Busuladžić, D. B. Milošević, and W. Becker, Phys. Rev. Lett. **103**, 043001 (2009).
[49] A. Gazibegović-Busuladžić, E. Hasović, M. Busuladžić, D. B. Milošević, F. Kelkensberg, W. K. Siu, M. J. J. Vrakking, F. Lépine, G. Sansone, M. Nisoli, I. Znakovskaya, and M. F. Kling, Phys. Rev. A **84**, 043426 (2011).
[50] W. Quan, X.-Y. Lai, Y.-J. Chen, C.-L. Wang, Z.-L. Hu, X. J. Liu, X.-L. Hao, J. Chen, E. Hasović, M. Busuladžić, W. Becker, and D. B. Milošević, Phys. Rev. A **88**, 021401(R) (2013).
[51] G. G. Paulus, W. Becker, and H. Walther, Phys. Rev. A **52**, 4043 (1995).
[52] D. B. Milošević and F. Ehlotzky, J. Phys. B **31**, 4149 (1998); **32**, 1585 (1999).